Light: Science & Applications (2015) 4, e284; doi:10.1038/lsa.2015.57
© 2015 CIOMP. All rights reserved 2047-7538/15
www.nature.com/lsa

ORIGINAL ARTICLE

Tunable and switchable polarization rotation with non-reciprocal plasmonic thin films at designated wavelengths

Dominik Floess[1], Jessie Y Chin[1], Akihito Kawatani[1], Daniel Dregely[1], Hanns-Ulrich Habermeier[2], Thomas Weiss[1] and Harald Giessen[1]

We experimentally demonstrate an ultra-thin plasmonic optical rotator in the visible regime that induces a polarization rotation that is continuously tunable and switchable by an external magnetic field. The rotator is a magneto-plasmonic hybrid structure consisting of a magneto-optical EuSe slab and a one-dimensional plasmonic gold grating. At low temperatures, EuSe possesses a large Verdet constant and exhibits Faraday rotation, which does not saturate over a regime of several Tesla. By combining these properties with plasmonic Faraday rotation enhancement, a large tuning range of the polarization rotation of up to 8.4° for a film thickness of 220 nm is achieved. Furthermore, through experiments and simulations, we demonstrate that the unique dispersion properties of the structure enable us to tailor the wavelengths of the tunable polarization rotation to arbitrary spectral positions within the transparency window of the magneto-optical slab. The demonstrated concept might lead to important, highly integrated, non-reciprocal, photonic devices for light modulation, optical isolation, and magnetic field optical sensing. The simple fabrication of EuSe nanostructures by physical vapor deposition opens the way for many potentially interesting magneto-plasmonic systems and three-dimensional magneto-optical metamaterials.
Light: Science & Applications (2015) **4,** e284; doi:10.1038/lsa.2015.57; published online 8 May 2015

Keywords: active tuning; Faraday rotation; magneto-optics; non-reciprocity; optical rotator

INTRODUCTION

A static magnetic field can alter the electromagnetic properties of materials and the way they interact with light. Depending on the actual material composition and nanostructure, such an interaction can give rise to non-trivial effects on the microscale or even the sub-microscale. For instance, an external magnetic field is capable of changing the rotation of polarization by a thin layer of magneto-optical material, which is termed the Faraday effect in transmission geometry[1,2] and polar Kerr effect in reflection geometry.[3–6] Such a magnetic field can also influence the intensity of light transmitted and reflected in scenarios of the transverse magneto-optical Kerr effect[7–9] and longitudinal magneto-photonic intensity effect.[10] Applying a magnetic field to magneto-optical materials can also change the nonlinear optical effects of the material.[11–15] These physical effects provide us with versatile approaches to develop magnetically tunable devices.[16,17]

In optical applications, the Faraday effect proves to be a versatile mechanism to manipulate light. When light travels through a magneto-optical medium, the induced polarization rotation θ is given for small magnetic fields by

$$\theta = v \cdot l \cdot B \tag{1}$$

where l is the optical path length, B is the magnetic field component in the propagation direction and v is the material specific Verdet constant. The magnetic-field-dependent Faraday rotation angle can be directly utilized in magnetic field sensing[18,19] and optical modulation.[20] In contrast to optical activity[21] the Faraday rotation is a non-reciprocal[22,23] polarization rotation effect. This fact means that the sign of the rotation is always relative to the direction of the magnetic field, whereas optically active media rotate the polarization relative to the direction of the wave vector. This property leads to the most prominent application of Faraday rotators, i.e., as core elements in optical isolators. These devices realize one-way light propagation to suppress parasitic feedback in a multitude of optical systems, including optical telecommunication networks[24–26] and laser systems.[27–29] In addition, systems with less restricted symmetry properties that exhibit asymmetric transmission of light (both in a reciprocal and non-reciprocal manner) have gained considerable attention recently.[30–32]

In the applications mentioned above, there is a strong trend toward highly integrated, tunable devices that demand dramatically downsized Faraday rotators. For the visible and standard telecommunication wavelengths in particular, the thickness of available Faraday rotators typically based on Bismuth-doped iron garnet (BIG) thick

[1]4th Physics Institute and Research Center SCOPE, University of Stuttgart, 70550 Stuttgart, Germany and [2]Max Planck Institute for Solid State Research, 70569 Stuttgart, Germany
Correspondence: D Floess, 4th Physics Institute and Research Center SCOPE, University of Stuttgart, Pfaffenwaldring 57, 70550 Stuttgart, Germany
E-mail: d.floess@pi4.uni-stuttgart.de
H Giessen, 4th Physics Institute and Research Center SCOPE, University of Stuttgart, Pfaffenwaldring 57, 70550 Stuttgart, Germany
E-mail: h.giessen@pi4.uni-stuttgart.de
Received 16 October 2014; revised 3 February 2015; accepted 4 February 2015; accepted article preview online 5 February 2015

films[33] is on the order of centimeters.[34] This is due mainly to the fact that a minimum optical path length must be available to reach a desired rotation range according to Equation (1). In many optical systems, such as laser systems, the optical isolation devices are the components limiting device miniaturization.[35] All existing non-conventional approaches to achieve optical isolation with significantly smaller devices suffer from large insertion losses.[25,26] Furthermore, the magnetic tunability of Faraday rotators is often limited by the saturation of Faraday rotation for an increasing magnetic field. Thus, to achieve a Faraday rotator with a large tuning range, it is desirable to utilize a material with not only a large effective Verdet constant but also a high saturation magnetic flux density. Here, we demonstrate a novel magneto-plasmonic structure that is designed to provide both properties while simultaneously maintaining a small physical size.

In recent years, plasmons have proved capable of enhancing a number of magneto-optical effects,[4,5,8,9,36] which demonstrates their potential for ultra-thin magneto-optical devices. Using plasmons to enhance the Faraday effect has been proposed theoretically[37,38] and demonstrated experimentally.[36] The experimental demonstration suggested a hybrid plasmonic-dielectric waveguide,[39–41] consisting of a thin BIG film and an attached plasmonic grating, which realizes a sophisticated mechanism to enhance Faraday rotation. Here, we employ this mechanism and advance it to 220-nm-thick devices, which show five times greater polarization rotation than in previously reported experiments. In addition, we experimentally demonstrate active magnetic tuning of the polarization rotation. In contrast to BIG, the utilized waveguide material EuSe provides a stronger magneto-optical response and also allows much simpler fabrication, which enables the creation of three-dimensional (3D) magneto-plasmonic metamaterials. Furthermore, we demonstrate, for the first time, that the dispersion properties of such structures can be exploited to freely tailor the working wavelength of the structure within the transparency window of the magneto-optical material. This novel concept for an actively tunable thin-film optical rotator with a designated working wavelength will have important applications in highly integrated optical environments.

MATERIALS AND METHODS

A large Faraday rotation angle might seem to be contradictory to a thin-film rotator structure. However, the two aspects can be combined by making the rotator structure resonant. The non-reciprocity[22,23] of the Faraday effect allows light to accumulate rotation of the same sign and magnitude for both forward and backward propagation. This behavior means that when light propagates through a medium and is reflected in the backward direction, the accumulated Faraday rotation is twice the rotation of only one pass. This rotation can be enhanced even further by additional round-trips through the medium.

This principle is utilized in the magneto-plasmonic structure schematically depicted in Figure 1a. The structure consists of a EuSe slab waveguide and a gold wire grating on top. Both the magnetic field and wave vector of the incident light are assumed to point in the same direction and perpendicular to the EuSe film. Henceforth, the incident polarization parallel and perpendicular to the wires is referred to as transverse electric (TE) and transverse magnetic (TM), respectively.

The gold nano-wire grating has two functions. First, it acts as a waveguide coupler and allows normally incident light to couple into the slab waveguide modes. The wave vectors of these modes possess a significant component in the *z*-direction. In the picture of ray approximation, this scenario can be understood as light bouncing back and forth inside the magneto-optical film (Figure 1a) and accumulating the rotations of multiple round-trips. When light is eventually coupled out of the film due to a finite lifetime, the effective Faraday rotation is significantly larger than that for a bare film.

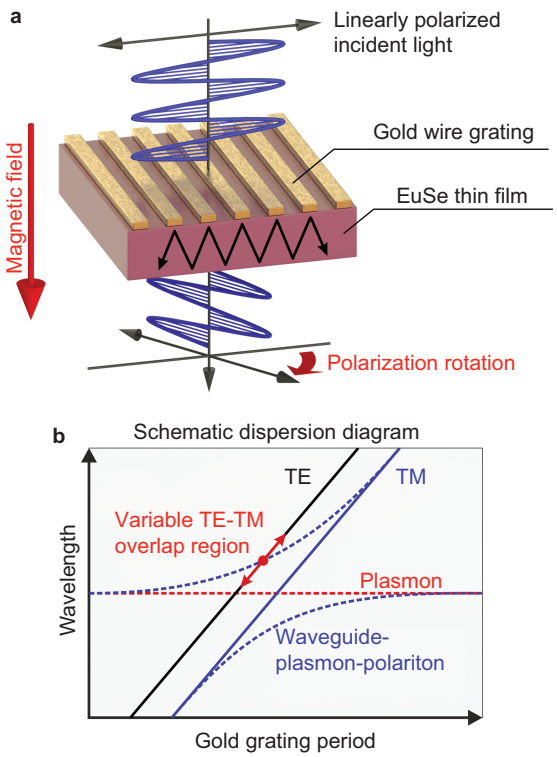

Figure 1 Illustration of the wavelength-specific Faraday rotation enhancement. (**a**) Geometry of the EuSe–Au hybrid structure. The applied magnetic field and incident light are normal to the EuSe film. There are two cardinal polarization orientations, namely, TE (electric field parallel to the gold wires) and TM (electric field perpendicular to the gold wires). Light coupled to the waveguide undergoes multiple round-trips through the EuSe slab and accumulates Faraday rotation. (**b**) Schematic dispersion graph of the hybrid structure. For TM-incident polarization, the plasmonic resonance of the gold wires couples strongly to the TM waveguide mode of the EuSe slab and forms a waveguide-plasmon-polariton. TE, transverse electric; TM, transverse magnetic.

Many applications require wavelength-specific device operation. The presented structure design provides the freedom to tune the working wavelength (i.e., the spectral region with largest rotation enhancement) to arbitrary positions within the transparency window of the magneto-optical film. To explain the principle behind the wavelength tunability, we must first consider the connection between Faraday rotation enhancement and the dispersion properties of the hybrid structure. The largest Faraday rotation enhancement occurs at wavelengths at which the structure supports both a TM-polarized and TE-polarized mode. In that case, the TM-to-TE conversion (i.e., polarization rotation) can occur most efficiently. The modes excited by TE- and TM-polarized incident light are themselves not purely (but mainly) TE- and TM-polarized due to the anisotropic permittivity tensor of the magneto-optical material. However, in the interest of readability, these modes are referred to here as TE and TM modes, respectively.

To overlap the TE and TM modes in *k*-space as well as at their energetic position, the second function of the metallic grating comes into play. In TM polarization, the gold wires provide a localized particle plasmon resonance that hybridizes with the TM waveguide

doi:10.1038/lsa.2015.57

mode[40] of the magneto-optical slab and forms a waveguide-plasmon-polariton (WPP). For the resulting TM-polarized WPP, there will then always exist a grating period such that its dispersion curve intersects with a TE waveguide dispersion curve at the same wavelength. This mechanism is illustrated in Figure 1b, which schematically displays the dispersion behavior of the magneto-plasmonic hybrid structure. The lines in the diagram trace the resonance frequencies of the TE and TM modes for different grating periods. The solid lines correspond to the case when the grating coupler is made of a dielectric material and thus does not support any plasmonic resonance. The dispersion for a metallic waveguide coupler is depicted as dotted lines. In the dielectric case, the TE and TM modes never overlap except for the zero grating period or inclined incidence,[39] whereas they overlap in the metallic case owing to the formation of the WPP. This effect occurs because, as a result of the coupling of the localized particle plasmon to the TM waveguide mode, the dispersion curve of the TM mode is bent over the TE waveguide-mode dispersion curve and an intersection is created.

The position of this intersection directly depends on the wavelength of the localized particle plasmon of the grating wires. By increasing (decreasing) the wire width of the grating, both the plasmonic resonance and intersection point of the TM and TE modes shift toward longer (shorter) wavelengths and larger (smaller) periods. Based on this feature, we will demonstrate the tuning of the working wavelength experimentally in the section on 'Results and discussion'.

A magneto-optical waveguide material with both a large Verdet constant and high saturation magnetic flux density was used to obtain a large tuning range of polarization rotation. In the 1960s, in the context of research on bubble memories, the group of Europium chalcogenides received attention for their exceptional magnetic properties and strong magneto-optical response at low temperatures.[42–44] In particular, the compound EuSe, which was used for the present structures, exhibits extremely large Faraday rotation angles on the order of 1 degree per Tesla and micrometer thickness in the visible wavelength range at temperatures of 30 K. EuSe also possesses a high saturation magnetic flux density of 2–5 T, depending on the wavelength.[42,44,45] Furthermore, the fabrication of EuSe thin films is very simple and was carried out by physical vapor deposition.[46] This feature is a significant advantage over BIG, which is widely utilized both in magneto-optical devices[33,34] and concept studies.[26,36,47] BIG films are typically fabricated by pulsed laser deposition[48] followed by high-temperature annealing, which is largely restricted to homogeneous films and does not allow for the direct incorporation of other materials, such as plasmonic nanostructures, into the film. With the flexibility of physical vapor deposition, EuSe provides the possibility of fabricating more sophisticated potential future designs, including 3D geometries, where the magneto-optical and plasmonic elements are merged. The gold gratings attached to the EuSe films were fabricated by electron beam lithography.[49]

The Faraday rotation measurements for the EuSe–Au hybrid structures were performed in a magnet cryostat at 30 K. The polarization rotation was measured with a rotating analyzer between the illuminated sample and a spectrometer. Because the present structures are anisotropic for rotation measurements, it is crucial that the incident light be either purely TE- or TM-polarized. For other incident polarizations, undesired reciprocal rotation contributions occur owing to different transmittances for TE and TM polarization. Wavelength-dependent deviations from the pure TE or TM polarizations can occur due to the Faraday rotation from glass elements within the reach of the magnetic field of the magnet cryostat. This behavior arises mainly as a result of cryostat windows and focusing lenses. For this reason, an intra-cryostat polarizer was placed directly in front of the sample. To avoid any Faraday rotation due to the glass components of the polarizer itself, a nanoparticle polarizer[50] was used when the polarizing metal particles were situated directly under the glass surface facing the sample.

The numerical simulations have been carried out by the Fourier modal method for anisotropic materials.[51] Our implementation is based on a scattering matrix algorithm[52] and has been improved by adaptive spatial resolution,[53] which allows us to derive the optical properties of metallo-dielectric systems efficiently. In addition to the calculation of far-field spectra, we used our *ab initio* method to derive the photonic resonances,[54] in which we search for the poles of the resulting scattering matrix on the complex frequency plane.

The gold has been described by tabulated data to calculate the far-field spectra.[55] The derivation of the photonic resonances requires an analytical continuation on the complex frequency plane, which has been achieved by the model described by Etchegoin *et al.*[56] For the substrate, we used a constant relative permittivity of epsilon=2.13. The diagonal elements of the permittivity tensor of the EuSe film were modeled using experimental data gained from transmission measurements of different plasmonic gratings on top of a EuSe slab. The off-diagonal elements of the dielectric tensor were obtained from measurements of a blank EuSe film at 30 K and 5 T, which is the condition given in the performed experiments.

RESULTS AND DISCUSSION

To support the principle of the Faraday rotation enhancement, the dispersion behavior of the demonstrated structures was simulated using the scattering matrix method. The simulations confirm the formation of WPPs in the EuSe–Au hybrid structure for TM incidence and also show that the maximum Faraday rotation enhancement can be expected around the intersection of the TE waveguide mode and TM-polarized WPP. The upper panels of Figure 2 show the simulated absorbance spectra for a 150-nm-thick EuSe film with a gold wire grating on top for varying the grating periods. The gold wires are assumed to be 70 nm thick and 70 nm wide. The black and white dashed lines trace the radiating TE- and TM-mode resonance frequencies of the EuSe hybrid structure and have been derived *ab initio* from the scattering matrix.[54] The non-radiating resonance modes are omitted. The diffraction induced Rayleigh anomaly[40] is plotted in red. For small periods, the TM hybrid-mode dispersion is dominated by the plasmonic resonance of the gold wires and is therefore relatively broad with a weak dependence on the grating period. For larger periods, the TM hybrid-mode dispersion becomes more waveguide-like and converges toward a sharp and purely waveguide-induced resonance. Because the localized particle plasmons in the gold wires can be excited only for TM-incident polarization, the TE-mode dispersion shows a distinct feature of a waveguide resonance. The corresponding Faraday rotation spectra are shown in the lower panels of Figure 2. The maximum Faraday rotation occurs around the intersection of the TE and TM mode dispersion, as predicted from the discussion in the previous section. For the case when the wave vector of the incident light is tilted, the dispersion behavior changes according to the discussion by Christ *et al.*[39,40] for non-magneto-optical hybrid structures. However, the criterion for maximum Faraday rotation enhancement remains unchanged: it occurs where the TM WPP has the strongest overlap with the TE waveguide modes. More discussion on that matter can be found in the supplement of the article. There, we also elaborate on the influence of the waveguide thickness and provide additional simulations.

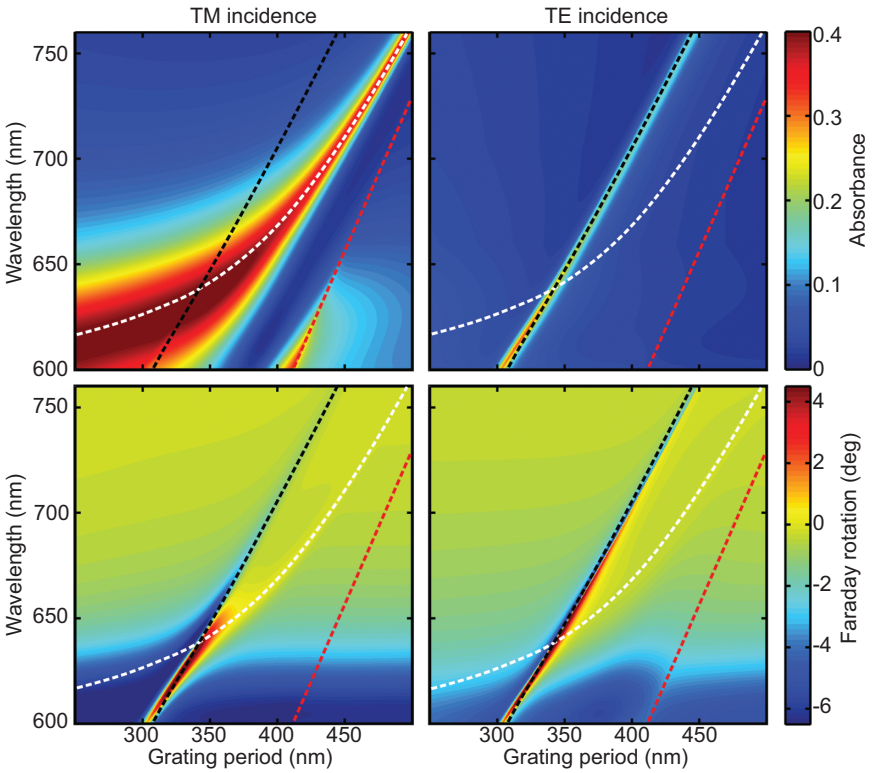

Figure 2 Simulation of absorbance and Faraday rotation for a 150-nm-thick EuSe slab and 70-nm-thick and 70-nm-wide periodic gold wires. The assumed conditions are a temperature of 30 K and a magnetic field of 5 T. The black and white dashed lines denote the calculated TE and TM resonance modes. The largest Faraday rotation occurs at the point where TM and TE modes overlap. The red dashed line indicates the Rayleigh anomaly, which is dependent on the grating period. TE, transverse electric; TM, transverse magnetic.

The simulated dispersion behavior for normal incidence was subsequently confirmed experimentally. Figure 3a displays transmittance and Faraday rotation spectra for TM incidence for different grating periods. The corresponding spectra from the simulations are plotted in Figure 3b. The black curves represent the case of a blank film without grating. The blue curves correspond to a 360-nm grating period and represent the case where the TE- and TM-mode dispersions have the greatest overlap. Hence, the largest Faraday rotation enhancement is achieved. At 662 nm, the structure exhibits a Faraday rotation of 4.2° at reasonably high transmittance of 30%. The other curves show that when the period is increased, the enhancement of the rotation decreases as the TE and TM modes move farther apart. As in the color-coded absorbance diagram in Figure 2, the resonance features of the TE mode (negative rotation contribution) and TM mode (positive rotation contribution) are drifting away from each other with an increasing grating period while simultaneously flattening out. The simulated and experimental data correspond well, although there is a difference in the Faraday rotation baseline plotted in black. This discrepancy is caused by the limited temperature accuracy of our cryostat system. In principle, this effect can be completely eliminated by using a cryostat that can maintain a temperature below 7 K, which is the Néel temperature of EuSe, below which the magneto-optical rotation is maximum and temperature independent. Earlier measurements (not shown here) confirmed that in this temperature range, the Faraday rotation of EuSe is even larger and not temperature-dependent.

As explained in the previous section, the Faraday rotation of the waveguide material can be enhanced at selected wavelengths. The only requirement is that the material offers a sufficiently low absorption at the wavelength of interest to achieve a high-quality factor of the waveguide resonator. From the visible to the near infrared, EuSe is transparent at wavelengths larger than 550 nm.[57] Figure 4 shows the measured Faraday rotation spectrum of a 150-nm-thick EuSe film at a temperature of 30 K and a magnetic flux density of 5 T. The black curve denotes the Faraday rotation for the case without plasmonic enhancement. Around the material resonance at 550 nm, EuSe shows largest Faraday rotation, which decreases toward the near-infrared spectral region while approaching a non-zero value. By tailoring the plasmonic gratings such that the TE waveguide mode and TM WPP mode dispersions overlap at different wavelengths, the Faraday rotation can be enhanced selectively at these tailored wavelengths. In the section on 'Materials and methods', it was shown that for a given thickness of the magneto-optical slab, this overlap can be achieved by just tuning the wire width and period of the metal wires. The colored curves in Figure 4 correspond to three different plasmonic gratings, which fulfill the TE–TM-matching condition. All gratings share a constant wire thickness of 70 nm. Both the wire width w=(70 nm, 80 nm, 90 nm) and the grating period p=(360 nm, 390 nm, 420 nm) are increasing from left to right. The resulting maximum absolute values of Faraday rotation are located at the wavelengths λ=(662 nm, 695 nm, 736 nm). For longer wavelengths, both the intrinsic Faraday rotation of the film and the enhanced rotation are decreasing. This finding is in agreement with the assumption that the enhanced Faraday rotation and the intrinsic Faraday rotation of a film are approximately proportional to each other for constant absorption, a constant waveguide coupling efficiency, and thus, a constant quality factor.

doi:10.1038/lsa.2015.57

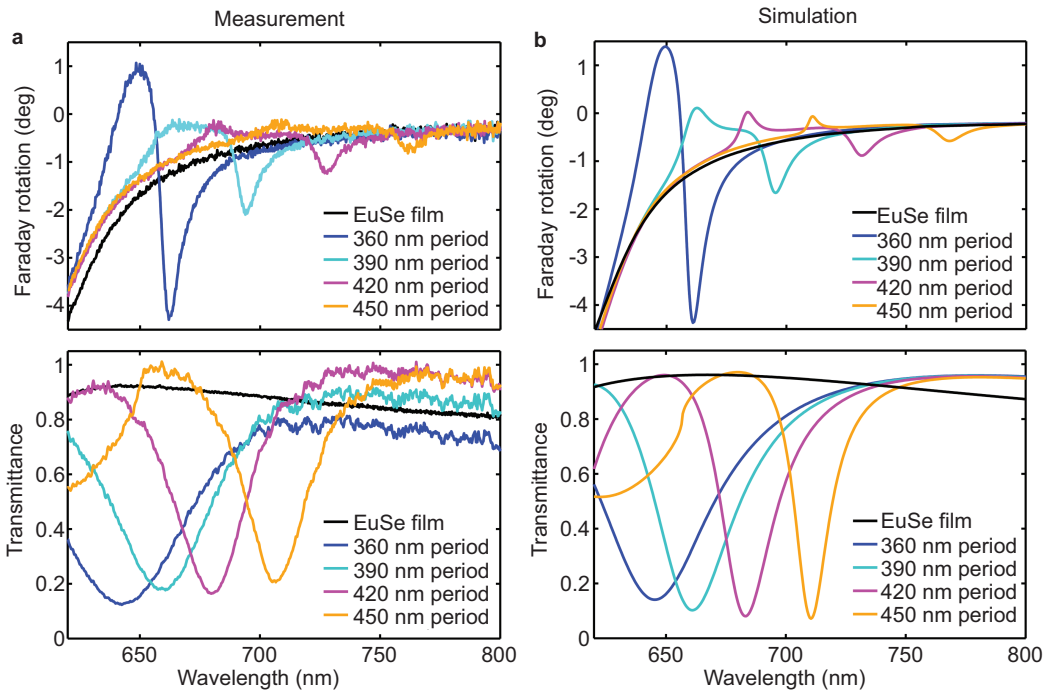

Figure 3 Faraday rotation and transmittance spectra for a 150-nm-thick EuSe slab and 70-nm-thick and 70-nm-wide periodic gold wires. The overlap of TM and TE waveguide mode can be successively increased and the Faraday rotation enhanced by varying the grating period. (**a**) Measured data. (**b**) Simulated data. TE, transverse electric; TM, transverse magnetic.

The magnetic field dependence of the Faraday rotation was measured to demonstrate the polarization tuning capability of the demonstrated EuSe–Au structures. Figure 5a shows the Faraday rotation of the structure with a 360-nm grating period, 70-nm wire thickness and 70-nm wire width for TM incidence. The magnetic field was varied from −5 T to +5 T. The structure geometry yields largest Faraday rotation at 663 nm. For this wavelength, a polarization rotation tuning range from −4.2° to +4.2° is obtained. The tuning behavior is nearly linear in the magnetic field, as can be extracted from Figure 5b. The polarization rotation measurement for inverted magnetic fields also acts as a control experiment to reveal potential spurious non-magnetically induced contributions. As discussed in the section on 'Materials and methods', due to the sample anisotropy, such effects can occur when the incident polarization deviates from an exactly TE or TM polarized state, for instance, as a result of the Faraday rotation of the cryostat windows. The highly mirror symmetric behavior of the measured rotation spectra in Figure 5a clearly shows that polarization errors of the incident light are well under control and sufficiently small.

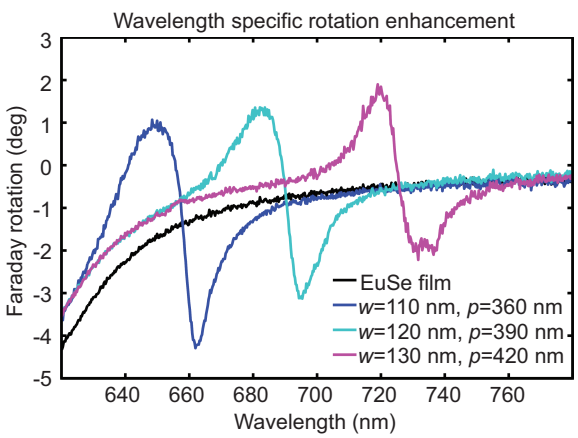

Figure 4 Experimental demonstration of sweeping the Faraday rotation enhancement over a range of wavelengths. The graph shows the Faraday rotation of a 150-nm-thick EuSe slab and 70-nm-thick periodic gold wires. From left to right, the curves correspond to a wire width *w* of (70, 80, 90 nm) and a grating period *p* of (360, 390, 420 nm).

CONCLUSIONS

We experimentally and theoretically demonstrated an actively tunable thin-film optical rotator with a variable working wavelength. To this end, we combined a slab of EuSe that possesses a large Verdet constant and high saturation magnetic flux density with an intelligent plasmonic grating design. The resulting structures exhibit special dispersion properties that allow for the overlap of TE- and TM-polarized eigenmodes to obtain significant Faraday rotation enhancement at designated wavelengths. The wavelength of interest can be selected by tuning the grating period and grating wire width. The magnitude of optical rotation can be magnetically tuned over a wide angular range and exhibits a nearly linear behavior of rotation with applied field. At 30 K for a 220-nm-thick structure, a rotation tuning range of up to 8.4° was obtained. For the present structure, this range can presumably be doubled when cooling down to temperatures below the Néel temperature of EuSe, which is 7 K.

We expect the demonstrated concept to have applications in highly integrated optics, demanding actively controlled optical modulation,[20] magnetic field sensing[18,19] and optical isolation.[24–29] Furthermore, the presented structure geometry is suitable for large-area fabrication,[58,59] which makes it a promising candidate design for non-reciprocal coatings of optical elements, such as lenses, with active external control at specific wavelengths. In addition, the direct attachment onto optical

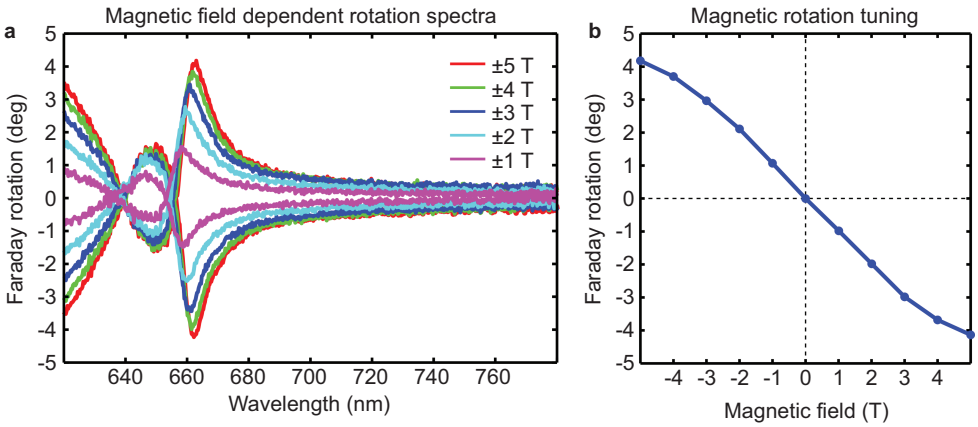

Figure 5 Magnetic tuning of the polarization rotation. (**a**) Faraday rotation of a 150-nm-thick EuSe slab and 70-nm-thick and 70-nm-wide periodic gold wires for different applied magnetic fields. (**b**) Rotation tuning curve at the maximum rotation angle of 4.2°.

fiber ends[60–62] or onto laser diodes could yield devices with extremely small volumes for a highly integrated environment.

The working principle of the presented structures is not restricted to EuSe as a waveguide material. It can be directly transferred to other magneto-optical materials. The only requirement is that the magneto-optical material provides a transparency window near the wavelength region of interest and a sufficiently high surface quality to ensure a high quality factor. These requirements can be met by commonly used room temperature magneto-optical materials, such as BIG,[48] yttrium iron garnet (YIG)[48] or terbium gallium garnet (TGG).[63] For the low-temperature regime, there are also other chalcogenides, such as EuS,[42] EuTe[44] and EuO,[64] which have similar magneto-optical properties as EuSe. The temperature at which these materials show the largest Faraday rotation can possibly be increased by doping with Gd. For example, alloying EuO with Gd can raise the Curie temperature from 69 K to 135 K.[65,66] EuSe and EuS combine large magneto-optical response, high saturation magnetic flux density, and simple thin-film fabrication *via* physical vapor deposition. Thus, they are promising materials for further magneto-plasmonic studies with structures that are not restricted to designs including strictly continuous magneto-optical films, as required for true 3D structures.

ACKNOWLEDGEMENTS

We gratefully acknowledge the funding by DFG (SPP1391, FOR730, and GI 269/11-1), BMBF (FARADAY, FKZ 13N12443), MWK, Baden-Württemberg Stiftung and ERC (ComplexPlas). JYC and DD also acknowledge support from Carl-Zeiss-Stiftung. We gratefully thank Jürgen Weis at the Max Planck Institute for Solid State Research in Stuttgart for providing cleanroom and electron beam lithography facilities. We also thank Yvonne Link (MPI FKF Stuttgart) for the thin-film evaporation and Michael Fronk and Peter Robaschik (TU Chemnitz) for help with initial low-temperature measurements. We thank the companies Toptica Photonics AG and Thorlabs GmbH for the helpful discussions on commercially availible optical isolators.

1 Körner T, Heinrich A, Weckerle M, Roocks P, Stritzker B. Integration of magneto-optical active bismuth iron garnet on nongarnet substrates. *J Appl Phys* 2008; **103**: 07B337.
2 Kahl S, Grishin AM. Evolution of properties of epitaxial bismuth iron garnet films with increasing thickness. *J Magn Magn Mater* 2004; **278**: 244–255.
3 Višňovský Š, Pařízek V, Nývlt M, Kielar P, Prosser V *et al*. Magneto-optical Kerr spectra of nickel. *J Magn Magn Mater* 1993; **127**: 135–139.
4 Sepúlveda B, González-Díaz JB, García-Martín A, Lechuga LM, Armelles G. Plasmon-induced magneto-optical activity in nanosized gold disks. *Phys Rev Lett* 2010; **104**: 147401.
5 González-Díaz JB, Sepúlveda B, García-Martín A, Armelles G. Cobalt dependence of the magneto-optical response in magnetoplasmonic nanodisks. *Appl Phys Lett* 2010; **97**: 043114.
6 Feng HY, Luo F, Kekesi R, Granados D, Meneses-Rodríguez D *et al*. Magnetoplasmonic nanorings as novel architectures with tunable magneto-optical activity in wide wavelength ranges. *Adv Opt Mater* 2014; **2**: 612–617.
7 Penfold C, Collins RT, Tufaile AP, Souche Y. Transverse magneto-optical Kerr effect: the phase change of reflected light. *J Magn Magn Mater* 2002; **242–245**: 964–966.
8 Belotelov VI, Akimov IA, Pohl M, Kotov VA, Kasture S *et al*. Enhanced magneto-optical effects in magnetoplasmonic crystals. *Nat Nanotechnol* 2011; **6**: 370–376.
9 Kreilkamp LE, Belotelov VI, Chin JY, Neutzner S, Dregely D *et al*. Waveguide-plasmon polaritons enhance transverse magneto-optical kerr effect. *Phys Rev X* 2013; **3**: 041019.
10 Belotelov VI, Kreilkamp LE, Akimov IA, Kalish AN, Bykov DA *et al*. Plasmon-mediated magneto-optical transparency. *Nat Commun* 2013; **4**: 2128.
11 Pavlov VV, Pisarev RV, Kirilyuk A, Rasing T. Observation of a transversal nonlinear magneto-optical effect in thin magnetic garnet films. *Phys Rev Lett* 1997; **78**: 2004–2007.
12 Kaminski B, Lafrentz M, Pisarev RV, Yakovlev DR, Pavlov VV *et al*. Spin-induced optical second harmonic generation in the centrosymmetric magnetic semiconductors EuTe and EuSe. *Phys Rev Lett* 2009; **103**: 057203.
13 Lafrentz M, Brunne D, Kaminski B, Pavlov VV, Henriques AB *et al*. Optical third-harmonic spectroscopy of the magnetic semiconductor EuTe. *Phys Rev B* 2010; **82**: 235206.
14 Lafrentz M, Brunne D, Kaminski B, Pavlov VV, Pisarev RV *et al*. Optical third harmonic generation in the magnetic semiconductor EuSe. *Phys Rev B* 2012; **85**: 035206.
15 Matsubara M, Schmehl A, Mannhart J, Schlom DG, Fiebig M. Giant third-order magneto-optical rotation in ferromagnetic EuO. *Phys Rev B* 2012; **86**: 195127.
16 Davoyan AR, Engheta N. Nonreciprocal rotating power flow within plasmonic nanostructures. *Phys Rev Lett* 2013; **111**: 047401.
17 Davoyan AR, Engheta N. Nanoscale plasmonic circulator. *New J Phys* 2013; **15**: 083054.
18 Sun L, Jiang S, Marciante JR. All-fiber optical magnetic-field sensor based on Faraday rotation in highly terbium-doped fiber. *Opt Express* 2010; **18**: 5407–5412.
19 Deeter MN, Rose AH, Day GW. Fast, sensitive magnetic-field sensors based on the Faraday effect in YIG. *J Light Technol* 1990; **8**: 1838–1842.
20 Ross WE, Psaltis D, Anderson RH. Two-dimensional magneto-optic spatial light modulator for signal processing. *Opt Eng* 1983; **22**: 224485.
21 Zhang S, Zhou JF, Park YS, Rho J, Singh R *et al*. Photoinduced handedness switching in terahertz chiral metamolecules. *Nat Commun* 2012; **3**: 942.
22 de Hoop AT. A reciprocity theorem for the electromagnetic field scattered by an obstacle. *Appl Sci Res Sect B* 1960; **8**: 135–140.
23 Potton RJ. Reciprocity in optics. *Rep Prog Phys* 2004; **67**: 717–754.
24 Shirasaki M, Asama K. Compact optical isolator for fibers using birefringent wedges. *Appl Opt* 1982; **21**: 4296–4299.
25 Bi L, Hu JJ, Jiang P, Kim DH, Dionne GF *et al*. On-chip optical isolation in monolithically integrated non-reciprocal optical resonators. *Nat Photonics* 2011; **5**: 758–762.
26 Fan L, Wang J, Varghese LT, Shen H, Niu B *et al*. An all-silicon passive optical diode. *Science* 2012; **335**: 447–450.
27 Ikushima I, Maeda M. Self-coupled phenomena of semiconductor lasers caused by an optical fiber. *IEEE J Quantum Electron* 1978; **14**: 331–332.
28 Morikawa T, Mitsuhashi Y, Shimada J, Kojima Y. Return-beam-induced oscillations in self-coupled semiconductor lasers. *Electron Lett* 1976; **12**: 435–436.
29 Petermann K. External optical feedback phenomena in semiconductor lasers. *IEEE J Sel Top Quantum Electron* 1995; **1**: 480–489.

doi:10.1038/lsa.2015.57

30 Menzel C, Helgert C, Rockstuhl C, Kley EB, Tünnermann A *et al*. Asymmetric transmission of linearly polarized light at optical metamaterials. *Phys Rev Lett* 2010; **104**: 253902.
31 Fan SH, Baets R, Petrov A, Yu ZF, Joannopoulos JD *et al*. Comment on ''Nonreciprocal light propagation in a silicon photonic circuit''. *Science* 2012; **335**: 38.
32 Zhou Y, Dong YQ, Fan RH, Hu Q, Peng RW *et al*. Asymmetric transmission of terahertz waves through a graphene-loaded metal grating. *Appl Phys Lett* 2014; **105**: 041114.
33 IntegratedPhotonics.com. Magneto-Optic LPE Garnet Faraday Rotator Crystals. Available at http://integratedphotonics.com/products/bigfaradayrotators.html (accessed 23 July 2014).
34 Thorlabs online catalog. Available at http://www.thorlabs.de (accessed 23 July 2014).
35 Liu M, Zhang X. Plasmon-boosted magneto-optics. *Nat Photonics* 2013; **7**: 429–430.
36 Chin JY, Steinle T, Wehlus T, Dregely D, Weiss T *et al*. Nonreciprocal plasmonics enables giant enhancement of thin-film Faraday rotation. *Nat Commun* 2013; **4**: 1599.
37 Belotelov VI, Doskolovich LL, Zvezdin AK. Extraordinary magneto-optical effects and transmission through metal-dielectric plasmonic systems. *Phys Rev Lett* 2007; **98**: 077401.
38 Gevorkian Z, Gasparian V. Plasmon-enhanced Faraday rotation in thin films. *Phys Rev A* 2014; **89**: 023830.
39 Christ A, Tikhodeev SG, Gippius NA, Kuhl J, Giessen H. Waveguide-plasmon polaritons: strong coupling of photonic and electronic resonances in a metallic photonic crystal slab. *Phys Rev Lett* 2003; **91**: 183901.
40 Christ A, Zentgraf T, Kuhl J, Tikhodeev SG, Gippius NA *et al*. Optical properties of planar metallic photonic crystal structures: experiment and theory. *Phys Rev B* 2004; **70**: 125113.
41 Linden S, Kuhl J, Giessen H. Controlling the interaction between light and gold nanoparticles: selective suppression of extinction. *Phys Rev Lett* 2001; **86**: 4688–4691.
42 Suits JC, Argyle BE. Paramagnetic faraday rotation of EuSe. *J Appl Phys* 1965; **36**: 1251–1252.
43 Shen YR, Bloembergen N. Faraday rotation of rare-earth ions in CaF_2. II. Experiments. *Phys Rev* 1964; **133**: A515–A520.
44 Schoenes J, Wachter P. High field magneto-optical study of EuSe and EuTe. *Phys B+C* 1977; **89**: 155–158.
45 Suits JC, Argyle BE. Magnetic birefringence of EuSe. *Phys Rev Lett* 1965; **14**: 687–689.
46 Mahan JE. *Physical Vapor Deposition of Thin Films*. Weinheim: Wiley-VCH; 2000.
47 Fan SH. Nanophotonics: magnet-controlled plasmons. *Nat Photonics* 2010; **4**: 76–77.
48 Wehlus T, Körner T, Leitenmeier S, Heinrich A, Stritzker B. Magneto-optical garnets for integrated optoelectronic devices. *Phys Status Solidi A* 2011; **208**: 252–263.
49 Vieu C, Carcenac F, Pépin A, Chen Y, Mejias M *et al*. Electron beam lithography: resolution limits and applications. *Appl Surf Sci* 2000; **164**: 111–117.
50 Codixx ColorPol Polarizer. Prod. number VIS 052 AC3 005299, 2013.
51 Li LF. Fourier modal method for crossed anisotropic gratings with arbitrary permittivity and permeability tensors. *J Opt A: Pure Appl Opt* 2003; **5**: 345–355.
52 Tikhodeev SG, Yablonskii AL, Muljarov EA, Gippius NA, Ishihara T. Quasiguided modes and optical properties of photonic crystal slabs. *Phys Rev B* 2002; **66**: 045102.
53 Weiss T, Granet G, Gippius NA, Tikhodeev SG, Giessen H. Matched coordinates and adaptive spatial resolution in the Fourier modal method. *Opt Express* 2009; **17**: 8051–8061.
54 Weiss T, Gippius NA, Tikhodeev SG, Granet G, Giessen H. Derivation of plasmonic resonances in the Fourier modal method with adaptive spatial resolution and matched coordinates. *J Opt Soc Am A: Opt Image Sci Vis* 2011; **28**: 238–244.
55 Johnson PB, Christy RW. Optical constants of the noble metals. *Phys Rev B* 1972; **6**: 4370–4379.
56 Etchegoin PG, Le Ru EC, Meyer M. An analytic model for the optical properties of gold. *J Chem Phys* 2006; **125**: 164705.
57 Güntherodt G, Schoenes J, Wachter P. Optical constants of the Eu chalcogenides above and below the magnetic ordering temperatures. *J Appl Phys* 1970; **41**: 1083–1084.
58 Guo HC, Nau D, Radke A, Zhang XP, Stodolka J *et al*. Large-area metallic photonic crystal fabrication with interference lithography and dry etching. *Appl Phys B* 2005; **81**: 271–275.
59 Bagheri S, Giessen H, Neubrech F. Large-area antenna-assisted SEIRA substrates by laser interference lithography. *Adv Opt Mater* 2014; **2**: 1050–1056.
60 Wang X, Venugopal G, Zeng JW, Chen YN, Lee DH *et al*. Optical fiber metamagnetics. *Opt Express* 2011; **19**: 19813–19821.
61 Lin YB, Zou Y, Mo YY, Guo JP, Lindquist RG. E-beam patterned gold nanodot arrays on optical fiber tips for localized surface plasmon resonance biochemical sensing. *Sensors* 2010; **10**: 9397–9406.
62 Zeng X, Jradi S, Proust J, Bachelot R, Zhang ZP *et al*. Direct functionalization of an optical fiber by a plasmonic nanosensor. *Opt Lett* 2011; **36**: 2919–2921.
63 Dentz DJ, Puttbach RC, Belt RF. Terbium gallium garnet for Faraday effect devices. *AIP Conf Proc* 1974; **18**: 954–958.
64 Ahn KY, Suits JC. Preparation and properties of EuO films. *IEEE Trans Magn* 1967; **MAG-3**: 453–455.
65 Schoenes J, Wachter P. Exchange optics in Gd-doped EuO. *Phys Rev B* 1974; **9**: 3097–3105.
66 Shafer MW, McGuire TR. Studies of Curie-point increases in EuO. *J Appl Phys* 1968; **39**: 588–590.

This work is licensed under a Creative Commons Attribution-NonCommercial-ShareAlike 3.0 Unported License. The images or other third party material in this article are included in the article's Creative Commons license, unless indicated otherwise in the credit line; if the material is not included under the Creative Commons license, users will need to obtain permission from the license holder to reproduce the material. To view a copy of this license, visit http://creativecommons.org/licenses/by-nc-sa/3.0/

Supplementary information for this article can be found on the *Light: Science & Applications*' website (http://www.nature.com/lsa/).